A&A 469, 61–74 (2007)
DOI: 10.1051/0004-6361:20065301
© ESO 2007

Astronomy & Astrophysics

Clues to the nature of high-redshift O VI absorption systems from their lack of small-scale structure⋆,⋆⋆

S. Lopez[1], S. Ellison[2], S. D'Odorico[3], and T.-S. Kim[4,⋆⋆⋆]

[1] Departamento de Astronomía, Universidad de Chile, Casilla 36-D, Santiago, Chile
e-mail: slopez@das.uchile.cl
[2] University of Victoria, Dept. Physics & Astronomy, Elliott Building, 3800 Finnerty Rd, Victoria, V8P 1A1, British Columbia, Canada
e-mail: sarae@uvic.ca
[3] European Southern Observatory, Karl-Schwarzschild-Str. 2, 85748 Garching-bei-München, Germany
e-mail: sdodoric@eso.org
[4] Institute of Astronomy, Madingley Road, Cambridge CB3 0HA, UK

Received 28 March 2006 / Accepted 13 March 2007

ABSTRACT

We present results of the first survey of high-redshift ($\langle z \rangle \sim 2.3$) O VI absorption systems along parallel lines of sight toward two lensed QSOs. After a careful and well-defined search, we find ten intervening O VI systems – identified by the presence of the $\lambda\lambda$1031, 1037 doublet lines, H I, and in most cases C IV, Si IV, and C III – and eight candidate systems for which we do not detect H I nor other metals. We assess the veracity of these systems by applying a classification scheme. Within the errors, all O VI systems appear at the same redshift and have similar line strengths in front of both QSO images, whereas in most cases C IV or Si IV show more differences across the lines of sight, either in radial velocity or line strength. We conclude that (1) the coherence length of O VI must be much larger than $\approx 1\ h_{70}^{-1}$ kpc, and (2) an important fraction of the C IV absorbers may not reside in the same volume as O VI. Given the inhomogeneous character of the data – different S/N ratios and degrees of blending – we pay special attention to the observational errors and their impact on the above conclusions. Since Doppler parameters are consistent with photoionization, we propose a model in which C IV occurs in two different photoionized phases, one large, with characteristic sizes of a few hundred kpc and bearing O VI, and another one a factor of ten smaller and containing C III. This model is able to explain the various transverse differences observed in column density and kinematics. We apply the model successfully to 2 kinds of absorbers, with low and high metallicity. In the low-metallicity regime, [C/H]~ -2, we find that [C/O] ≈ -0.7 is required to explain the observations, which hints at late ($z \lesssim 6$) rather than early metal enrichment. In the high-metallicity regime, the observed dissociation between O VI and C IV gas might be produced by galactic outflows. Altogether, the relative abundances, inhomogeneous C IV and featureless O VI are consistent with gas that has been processed recently before the absorption occurred (thus close to star-forming regions). Finally, we discuss briefly three associated systems ($z_{\rm abs} \sim z_{\rm em}$) that also show O VI.

Key words. cosmology: observations – intergalactic medium – galaxies: halos – galaxies: quasars: absorption lines – quasars: individual: HE1104-1805 – quasars individual: RX J0911.4+0551

1. Introduction

Although once supposed to contain primordial material unenriched by the products of star formation, the Lyα forest is now well known to frequently exhibit associated metal lines. The most commonly detected metal feature at high redshift is the C IV doublet (e.g. Cowie & Songaila 1998; Ellison et al. 2000; Schaye et al. 2003; Aracil et al. 2004) due to the combination of its elemental abundance, convenient rest wavelength and ionization potential. Early models that used simple recipes for ionization corrections and assumed uniform metallicities determined that the carbon abundance was in the range of 10^{-2} to 10^{-3} of the solar value (e.g. Haehnelt et al. 1996; Davé et al. 1998). More sophisticated modeling has confirmed this result, and shown that the metallicity is most dependent on the gas overdensity, but largely insensitive to redshift in the range $2 < z < 4$ (Schaye et al. 2003). Although the low metallicities and relatively low $N_{\rm H\,I}$ column densities of the associated Lyα may hint toward an inter-galactic origin for C IV absorbers, recent work by Adelberger et al. (2003, 2005) has demonstrated a strong connection between the high column density C IV systems and Lyman break galaxies at $z \sim 3$. Indeed, Adelberger et al. (2005) infer that star-forming galaxies in their sample exhibit C IV absorption out to 80 kpc, sufficient to account for the bulk of observed absorbers (but note that these observations do not rule out an inter-galactic origin of the *weak* C IV absorbers detected with pixel-statistics techniques; Pieri et al. 2006).

With large datasets of high S/N spectra, extensive catalogs of other metal species such as Si IV (e.g., Aguirre et al. 2004) and O VI (e.g., Schaye et al. 2000; Carswell et al. 2002; Simcoe et al. 2002, 2004; Levshakov et al. 2003) are now becoming available. Species which represent a range of nucleosynthetic origins and ionization states allow us to probe a range of environments and

⋆ Based on observations made at the European Southern Observatory (ESO), under programs 67.A-0278(A) and 70.A-0439(A), with the UVES spectrograph at the VLT, Paranal, Chile.
⋆⋆ Appendix A and Table 3 are only available in electronic form at http://www.aanda.org
⋆⋆⋆ *Present address*: Astrophysikalisches Institut Potsdam, An der Sternwarte 16, 14482, Potsdam, Germany. e-mail: tkim@aip.de

Article published by EDP Sciences and available at http://www.aanda.org or http://dx.doi.org/10.1051/0004-6361:20065301

Table 1. VLT UVES observations of HE1104-1805 and RX J0911.4+0551.

QSO	UVES Setup	Wavelength [nm]	Exp. Time [s]	Observing Date	Seeing [arcsec]	$FWHM^a$ km s^{-1}	S/N(A)^b	S/N(B)^b
HE1104-1805	Dic- (390+580)	328–445, 476–684	7 600	Jun. 01	0.7–0.9	6.7	30, 90	15, 40
	Dic- (437+860)	376–500, 667–1040	40 020	Apr. 01–Jan. 02	0.5–1.0			
	Dic- (346+564)	305–390, 460, 660	11 400	Apr. 01–Jun. 01	0.5–0.8			
RX J0911.4+0551	Dic- (390+564)	328–445, 460–560, 567–660	43 200	Dec. 02–Feb. 03	0.7–1.1	7.0	40, 60	12, 20

[a] Resolution of final spectrum. [b] Median signal-to-noise ratio per pixel blue and redwards of Lyα emission.

physical states. For example, O VI is a particularly advantageous tracer of metals in the low density Lyα forest because it has the highest ionization fraction for $N_{\rm H\,I} \lesssim 10^{15}$ cm^{-2} (e.g. Schaye et al. 2000; Simcoe et al. 2004), and because oxygen is a cosmically abundant element. These O VI studies have inferred enrichment of 10^{-2}–10^{-3} $Z_\odot$ in IGM structures close to the mean density of the universe at $z \sim 2$. However, such widespread metal pollution is not necessarily indicative of in-situ Population III star enrichment. Indeed, a number of authors (e.g. Aguirre et al. 2001; Scannapieco et al. 2002; Simcoe et al. 2004) have modeled the contributions from Pop III stars versus galactic winds and concluded that the latter is the dominant enrichment source. The connection between O VI and galaxies has been strengthened further by correlations between color-selected galaxies (many with spectroscopic redshifts) and absorbers by Simcoe et al. (2006). Ionization modeling of these O VI absorbers, many of which exhibit a suite of other metal species such as N V, C III and Si III, led Simcoe et al. (2006) to conclude that the high metallicities, large coherence scales and small cloud sizes were consistent with material being expelled from galaxies, e.g. by supernova-driven winds. However, others have argued that early populations of massive stars contribute a significant fraction of the metals, up to 60% according to Qian & Wasserburg (2005).

Further clues to the origin and environment of O VI absorbers can be obtained through ionization modeling which can constrain densities and heating mechanisms. So far, many such studies have been executed at *low redshift*. For example, modeling the population of $z \lesssim 0.3$ O VI absorbers discovered by HST and FUSE have revealed predominantly collisionally ionized gas at $T \sim 10^5$ K (e.g. Tripp & Savage 2000; Tripp et al. 2000; Danforth & Shull 2005; Stocke et al. 2006), although multiphase models are often required (Danforth et al. 2005). The majority of low redshift O VI absorbers have therefore been associated with inter-galactic gas that is shock heated as it forms large scale structures, the so-called warm-hot intergalactic medium (WHIM). O VI has also now been detected in a large number of Galactic sightlines, both in the disk (e.g. Bowen et al. 2005) and in halo clouds (e.g. Savage et al. 2003), and in high-velocity clouds (Fox et al. 2006). The Galactic O VI absorbers have been associated with violent dynamical and non-equilibrium processes (Indebetouw & Shull 2004; Bowen et al. 2005). In contrast, high redshift O VI absorbers have so far almost universally been found to be photo-ionized (Bergeron et al. 2002; Carswell et al. 2002; Levshakov et al. 2003; but see Reimers et al. 2001; Simcoe et al. 2002).

The Adelberger et al. (2005) sizes of LBG metal enrichment are consistent with limits obtained from binary or gravitationally lensed QSOs which can be used to determine the transverse size of absorbers. A number of studies (e.g., Smette et al. 1995; Petitjean et al. 1998; Lopez et al. 2000; Rauch et al. 2001) have seen correlations on scales up to tens of kpc, but with fractional column density variation increasing up to 50% for 100 kpc separations (e.g. Fig. 11 in Ellison et al. 2004).

In this paper we combine the utility of gravitational lensing with ionization modeling to further investigate the physical state and coherence scale of O VI absorbers. This is the first time that a direct measure of O VI sizes from gravitational lensing has been achieved. We complement our coherence scale limits derived from lensing with models of one and two phase ionized media. The combination of constraints from these two directions allows us to derive approximate sizes (under certain assumptions of the multi-phase structure) and relevant abundances of C, N and O.

The targets that we use for this work are HE1104-1805 ($z_{\rm em} = 2.32$) and RX J0911.4+0551 ($z_{\rm em} = 2.80$). These objects have been studied extensively in the lensing literature and, in the case of HE1104-1805, studies on intervening absorption line systems also exist (of which the most pertinent to our study are: Smette et al. 1995; Lopez et al. 1999; Rauch et al. 2001). For RX J0911.4+0551, optical low-resolution spectra are reported in the discovery paper by Bade et al. 1997, and medium-resolution spectra more recently by Rauch et al. (2005); here we present the first high-resolution spectra. Both lens systems have transverse separations of $\approx 3''$. At the redshifts of the intervening systems studied here, the line-of-sight (LOS) separation ranges between $S = 0.2$ and 1.4 kpc, for a cosmology with $H_0 = 70$ km s^{-1} Mpc^{-1}, and $(\Omega_M, \Omega_\Lambda) = (0.3, 0.7)$.

The paper is organized as follows: after describing the observations in Sect. 2, in Sect. 3 we describe the selection method and the individual O VI absorption systems that were found, along with an assessment of sample completeness. In Sect. 4 we analyze observed properties of those systems across the lines of sight. In Sect. 5 we describe results and uncertainties from photoionization models. Finally, in Sect. 6 we compare observations and models to draw inferences about the origin of the high-redshift O VI gas. The conclusions are outlined in Sect. 7 and in the Appendix we describe the associated O VI systems.

2. Observations and data reduction

We observed both QSO systems with the VLT UV-Visual Echelle Spectrograph (UVES) in several runs from June 2001 through February 2003. Spectra of each QSO system were acquired simultaneously by aligning the slit with the 2 lensed images ("A" and "B"). This configuration is well defined for the double QSO HE1104-1805, but RX J0911.4+0551 is a quadruple system and what we shall call its "A" spectrum is actually the sum of three images (A1, A2, and A3 in Burud et al. 1998) which are not resolved in normal seeing conditions. Extraction of each 2-dimensional spectra was carried out with our own pipeline, which is based on simultaneous fitting of the spatial profiles (see Lopez et al. 2005, for details). For both QSO systems images A and B are separated by 3–4 seeing units, so the the fitting procedure ran smoothly. Table 1 lists the observational and spectrum-quality parameters.

Before coadding orders, the spectra were rebinned to a common vacuum-heliocentric scale with pixel size of 0.043 Å. The final spectral resolution in the coadded spectra was *FWHM* 6.7 and 7.0 km s^{-1}, for HE1104-1805 and RX J0911.4+0551, respectively. Finally, the coadded orders were normalized by dividing out the response function and QSO continuum simultaneously. The continuum was estimated first in the echelle orders of the A spectra by fitting cubic splines through featureless spectral regions. The continuum in QSO B (the faintest QSO component) was a scaled version of that of QSO A. Minor adjustments to the B continuum had to be made to account for differences in the flux ratios on top of emission lines. In RX J0911.4+0551, we have fitted out the mini-broad absorption system at $z = 2.57$ reported in Bade et al. (1997).

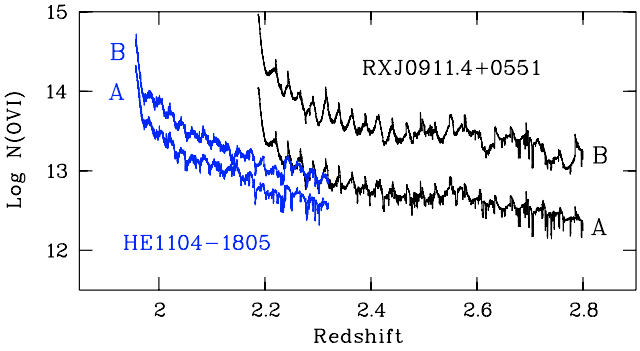

Fig. 1. Three-σ detection limits in terms of O VI column density for HE1104-1805 and RX J0911.4+0551.

3. Absorption systems

3.1. Selection

Since the main goal of this paper is to study LOS differences between O VI absorption systems and the spectra have disparate S/N ratios, the selection of the systems must be made as objective and unbiased as possible.

We have searched for O VI systems based on three independent methods, which we applied to each of the LOS *separately*:

1. Identify all Lyα lines with $N_{\rm H\,I} \gtrsim 10^{13.5}$ cm^{-2} (checking for Lyβ and Lyγ to avoid confusion with strong metal lines in the forest), then look for O VI at similar redshift within ±200 km s^{-1}. When an O VI candidate was found, check whether doublet lines could be Lyβ interlopers. Note that this $N_{\rm H\,I}$ cutoff includes systems for which O VI normally has not been detected by previous surveys. One caveat of the method is that it will fail to find highly ionized systems with no H I.
2. Identify C IV absorption systems and look for O VI at similar redshift.
3. Blindly search for O VI features taking into account the doublet ratio and possible forest blending. This method is limited to clean and high S/N parts of the forest, but it is advantageous in finding potential broad and shallow O VI absorbers. This search was performed down to $z > 2.0$ (HE1104-1805 A), $z > 2.1$ (HE1104-1805 B), $z > 2.2$ (RX J0911.4+0551 A), and $z > 2.5$ (RX J0911.4+0551 B), which correspond to 3σ detection limits for O VI of $\approx 10^{13.5}$ cm^{-2} (see Fig. 1).

We found twenty one candidate O VI systems. These are listed in Table 2. We then classified these candidates (column "class" in the table) according to the following criteria:

- Associated system: redshift is within $v < 3000$ km s^{-1} of the systemic QSO redshift.
- Class I: in both spectra both O VI doublet lines are detected at the 3σ significance level or better, and show the proper doublet ratios. Other metal species are present and $N_{\rm H\,I} > 10^{13.5}$ cm^{-2}.
- Class II: like Class I, but one of the O VI doublet lines is detected at low significance in either of the spectra, or other metal species are not detected.
- Class III: Like Class II but no metals are present and $N_{\rm H\,I} < 10^{13.5}$ cm^{-2}.

All these candidate systems are shown in Figs. 2 to 11 and A.1 to A.3. Associated systems are treated in the Appendix.

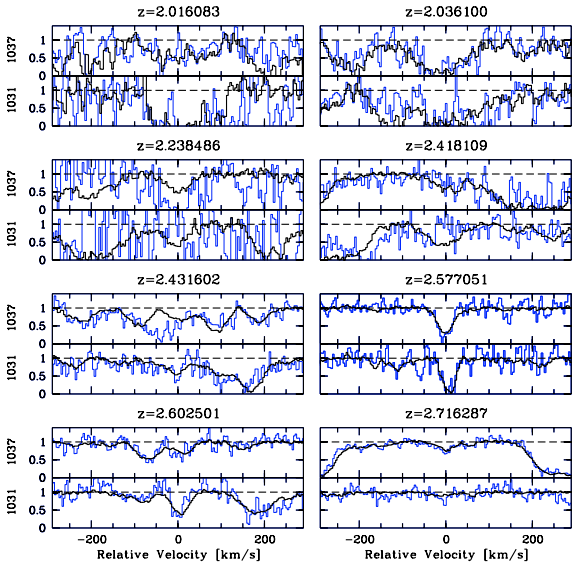

Fig. 2. Class III O VI systems toward HE1104-1805 and RX J0911.4+0551 (see Table 2). The thick black line corresponds to the A spectra; the thin blue one to the B spectra.

The class III absorbers represent the less certain identifications, all of which are shown in Fig. 2. Almost all of these were discovered by method 3, except the $z = 2.418109$ system toward RX J0911.4+0551. This candidate does show H I within ±200 km s^{-1}, but the 1037 line is also identified with 1031 of the Class I system at $z = 2.437271$, making the former identification uncertain. For the rest of Class III systems, and when the S/N is high enough, we note that an absorption feature at the position of O VI appears always in the two spectra. However, let us emphasize that in this sub-sample there is no clear, unblended case of O VI-only system. Consequently, the rest of this paper shall deal only with the ten remaining Class I and II systems.

3.2. Sample completeness

One check of sample completeness is to compare the number of selected systems with previous studies. To this end we count systems that are class I or II (since previous studies have considered systems with H I). For a total redshift path surveyed of $\Delta z = 0.649$ (based on O VI detectability in the lower S/N spectra of LOS B, which is one of the selection criteria), we find 7 systems with $W_{\rm rest} \geq 25$ mÅ. The estimated number density of O VI systems in our sample is thus $d\mathcal{N}/dz \approx 10.8 \pm 4.1$ at $\langle z \rangle = 2.3$. This density is consistent with previous estimates by

Table 2. Results of search for O VI systems toward HE1104-1805 and RX J0911.4+0551.

QSO	LOS A		LOS B		Class
	z_A	Method[a]	z_B	Method[a]	
HE1104-1805	2.314201	1, 2	2.314201	1, 2	Associated
	2.299304	1, 2	2.299304	1, 2	Associated
	2.200800	1, 2	2.200822	1, 2	II
	2.158112	1, 2	2.158139	1, 2	II
	2.086682	1, 2			II
			2.052440	2	II
	2.036100	3			III
	2.016083	3			III
	2.010473	2	2.010452	2	II
RX J0911.4+0551	2.776399	2	2.776399	2	Associated
			2.716287	3	III
	2.632495	1, 2	2.632495	1, 2	I
	2.626749	1			II
	2.623886	1			II
			2.602501	3	III
	2.577051	3	2.573192	3	III
	2.517045	1, 2	2.516961	2	I
	2.437271	1, 2	2.437265	2	I
	2.431602	3			III
	2.418109	1, 2	2.418124	1	III
	2.238486	3			III

[a] Method 1: H I as a signpost; method 2: C IV as a signpost; method 3: blind O VI search.

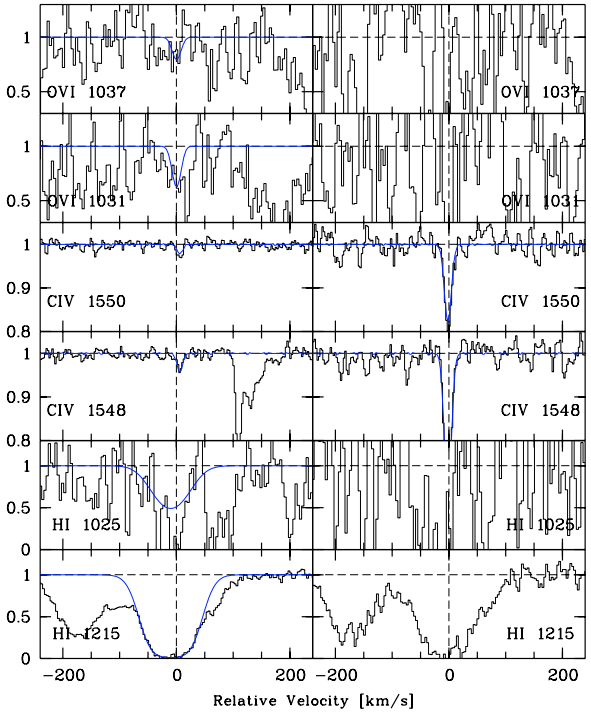

Fig. 3. Class II system in HE1104-1805. Lefthand (righthand) panels show transitions observed along sightline A (B). The smoothed lines show Voigt profiles with line parameters listed in Table 3. In both panels the vertical dashed line indicates $z = 2.010473$, which is the redshift of O VI in the A spectrum.

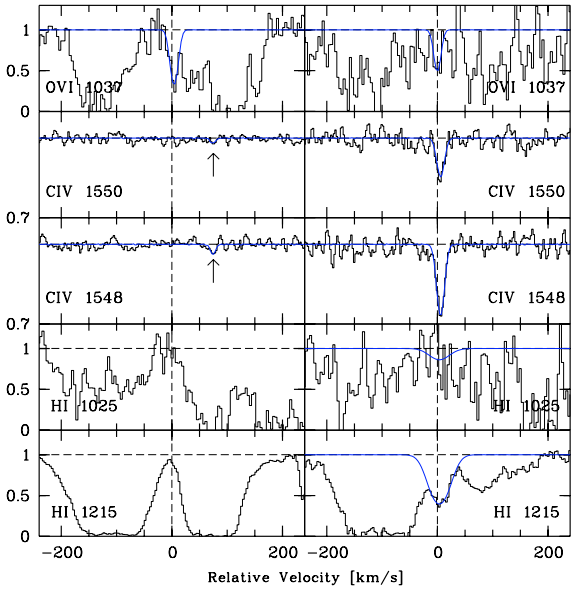

Fig. 4. Class II system in HE1104-1805. Panels and symbols as for Fig. 3, but for $z = 2.052440$, which is the redshift of O VI in the B spectrum. Arrows mark a possible C IV system in the A spectrum.

e.g., Carswell et al. (2002; $dN/dz \approx 11.4 \pm 4.0$) or Reimers et al. (2001), so our particular selection criteria do not seem to lead to a biased sample.

3.3. Line parameters

We used the FITLYMAN package in MIDAS to fit Voigt profiles[1] to class I and II systems. When not otherwise stated, the O VI, C IV and H I lines were fitted independently so that identical velocity is not a pre-requisite (except in Sect. 5 when we test photoionization models). Allowing the components' velocity to be a free parameter helps quantify the extent of these differences along and across the LOS. The $N_{\rm H\,I}$ was constrained only in a

[1] VPFIT was tried independently on several systems, yielding exactly the same results.

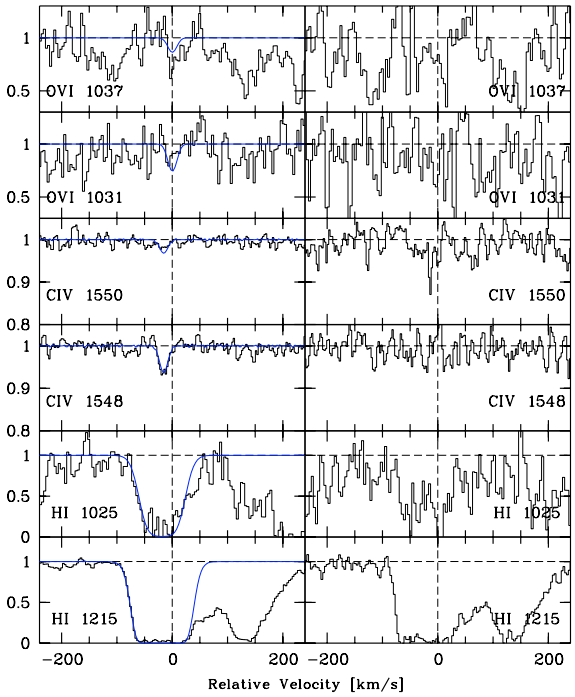

Fig. 5. Class II system in HE1104-1805. Panels and symbols as for Fig. 3, but for $z = 2.086682$.

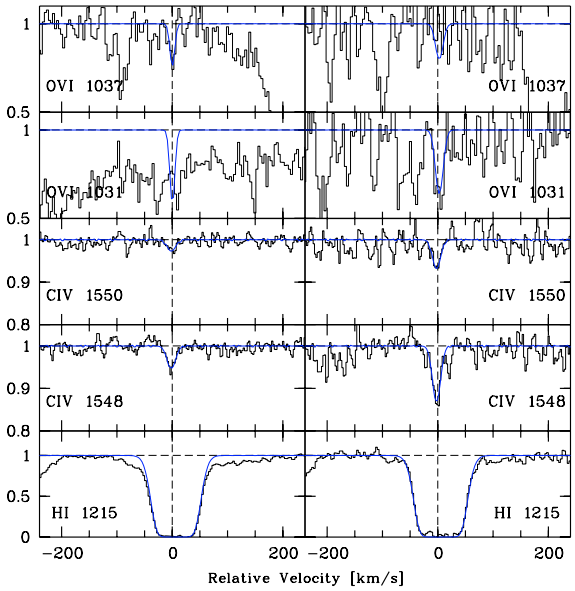

Fig. 6. Class II system in HE1104-1805. Panels and symbols as for Fig. 3, but for $z = 2.158112$.

few systems. In the much more modest S/N spectra of the B QSOs we attempted a fit only to O VI and C IV lines.

In Figs. 3 to 11 we show transitions for which we were able to obtain line constraints. The smoothed lines are the results of the fits and their parameters are listed in Table 3. The vertical dashed lines in the figures indicate in both panels the redshift of O VI along LOS A (except in Fig. 4). The transverse (proper) distance between LOS, $S(z)$, was calculated using Eq. (1) of Smette et al. (1992) and Eqs. (7) and (8) of Tzanavaris & Carswell (2003), and assuming QSO angular separations and lens redshifts $(\theta; z_{\rm lens}) = (3\farcs20; 0.73)$ and $(3\farcs06; 0.77)$, respectively for HE1104-1805 (Lidman et al. 2000) and RX J0911.4+0551 (Kneib et al. 2000).

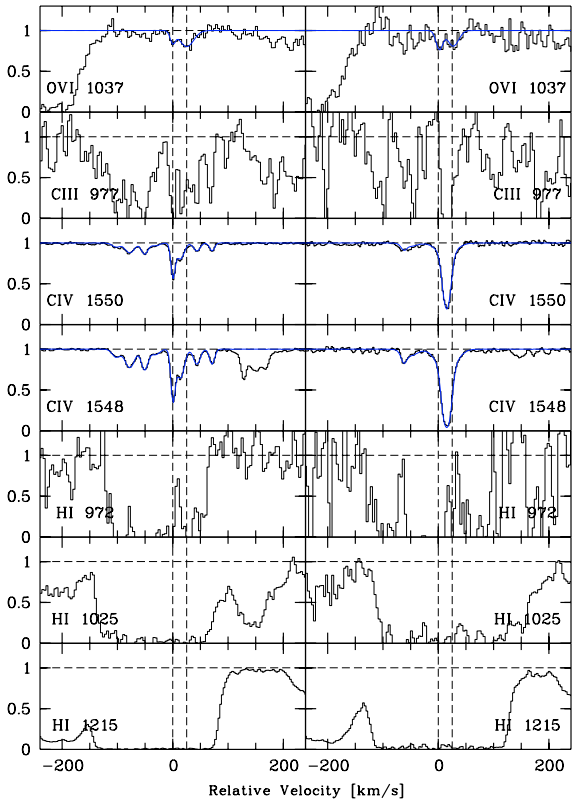

Fig. 7. Class II system in HE1104-1805. Panels and symbols as for Fig. 3, but for $z = 2.200800$ and $z = 2.201069$.

3.4. Description of Class I and II systems

$z = 2.010473$, $S = 1.8$ kpc, Class II system in HE1104-1805, see Fig. 3 This system was identified through the presence of C IV in both spectra, and absorption features at the position of both O VI doublet lines. The detection of O VI toward QSO A is based on the 1037 line, albeit at low significance level. At the position of O VI in B the spectrum is too noisy to attempt any line-profile fit. C IV can be fitted in both spectra and shows an order of magnitude variation in column density. H I is constrained in A by Lyα and Lyβ .

$z = 2.052440$, $S = 1.5$ kpc, Class II system in HE1104-1805, see Fig. 4 For this O VI system unfortunately only the 1037 lines are available. In the B spectrum, this line matches C IV and a weak ($N_{\rm H\,I} = 10^{14.5}$) H I line. C III is not covered. Surprisingly at such small LOS separations, the H I profile is quite different in the A spectrum: no H I is observed at the position of O VI and strong H I lying redwards has no counterpart in the B spectrum. There is a marginal (3σ in 1548) detection of C IV toward QSO A at $\approx$80 km s^{-1} that matches the strong H I system.

$z = 2.086682$, $S = 1.3$ kpc, Class II system in HE1104-1805, see Fig. 5 In this system the detection of O VI toward QSO A is based on both doublet lines albeit at low significance level. C IV is clearly detected but blueshifted by $\sim$14 km s^{-1}. H I is constrained in A by Lyα and Lyβ but both lines are saturated so we only get a lower limit on $N_{\rm H\,I}$. In B, from a non-detection of C IV, we get a 5σ limit $\log N({\rm C\,IV}) < 12.0$ cm^{-2}. At the position of O VI the spectrum is too noisy to attempt any line-profile fit.

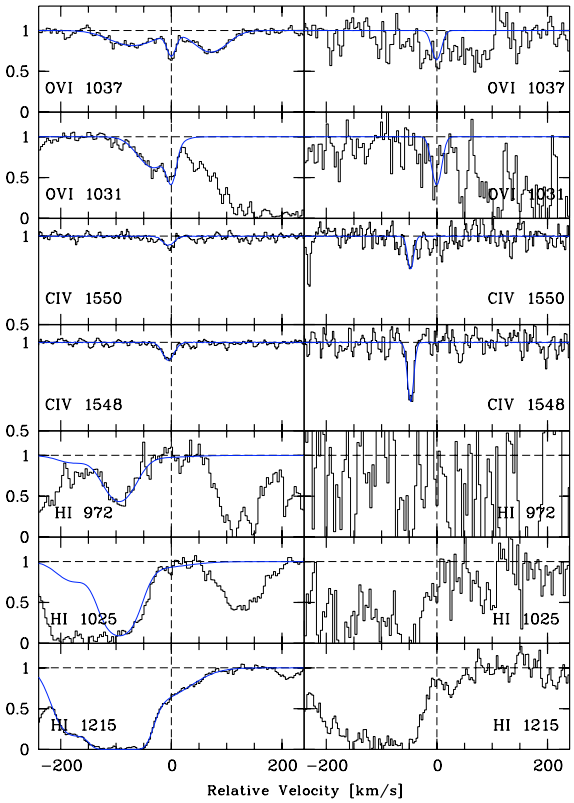

Fig. 8. Class I system in RX J0911.4+0551. Panels and symbols as for Fig. 3, but for $z = 2.437271$.

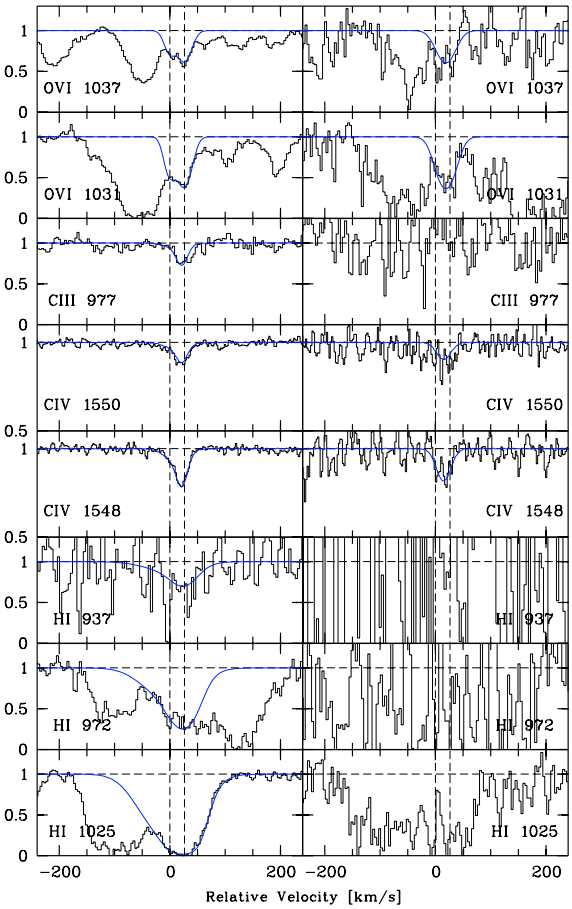

Fig. 9. Class I system in RX J0911.4+0551. Panels and symbols as for Fig. 3, but for $z = 2.516735$ and $z = 2.517045$.

$z = 2.158112$, $S = 0.9$ kpc, Class II system in HE1104-1805, see Fig. 6 For this system the detection of O VI is based on the 1037 line in A and the 1031 one in B (although the 1031 line in the latter is only a 3σ detection). In spectrum A there is a damped Lyα system at $z = 1.66$ that affects the continuum at the position of the 1031 line. C IV is clearly detected in both LOS. The redshifts are almost identical ($\Delta v \sim 2$ km s^{-1} according to the line centroids). H I is constrained in A and B only by saturated Lyα, so the $N_{\rm H\,I}$ estimates have to be taken as lower limits.

$z = 2.200800$, $S = 0.2$ kpc, Class II system in HE1104-1805, see Fig. 7 This is a Lyman-limit system (LLS) with rich structure in C III and C IV (also in Si IV, not shown in the figure). We note in the A spectrum that C III and C IV seem to follow each other, indicating that they arise in the same gas volume. A similar behavior is seen in B, although with some additional blending from interlopers. Note the $v \approx 30$ km s^{-1} offset between H I in A and B. The detection of O VI is based solely on the 1037 line in A because of Lyα forest blending. The system was included because in both LOS the redshift match with C IV is good and the small Doppler parameters indicate metal lines.

$z = 2.437271$, $S = 1.4$ kpc, Class I system in RX J0911.4+0551, see Fig. 8 In this system the two O VI doublet lines are clearly present in the A spectrum. Although blended with shallow Lyα (which have been included in the line fits), the doublet ratios are consistent with a positive identification. There is a good match in velocity between C IV and O VI. C III is unfortunately blended and therefore not constrained. From non-detection of N V we obtain the 3σ limit $\log N(\mathrm{N\,V}) < 12.2$ cm^{-2}. For H I, we have considered three components in the fit which yields reliable H I column densities given that the non-saturated Lyγ is available. The strong H I velocity component closest to O VI appears blue-shifted by $\sim$100 km s^{-1}. The component at $v = 0$ km s^{-1}, on the other hand, is weak and shallow, and has the largest Doppler parameter in the sample, $b = 71$ km s^{-1}.

In B, there is a clear C IV system, which appears blueshifted by 43 km s^{-1} with respect to C IV (and O VI) in A, although we cannot discard that undetected weak C IV lies exactly at the same redshift as in A. From the Lyα profile of B (Lyβ does not constrain H I and Lyγ is too noisy) we observe that H I does not vary between A and B, except for the flux excess at $v = 0$ km s^{-1} in LOS B. The presence of O VI in B is not conclusive; nevertheless a 1-component fit gives same column density as in A within the formal errors, and an almost identical b-value. Inclusion of Lyα blends in the fit was regarded as too complicated, given the noise level.

$z = 2.516735$ and $z = 2.517045$, $S = 1.0$ kpc, Class I system in RX J0911.4+0551, see Fig. 9 This O VI candidate also shows the correct line-strength ratio. We fit two velocity components in A, and note that C IV has also two components. The H I was constrained by a 2-component fit to Lyβ through Lyϵ, with redshifts fixed at the O VI values. C III is also detected, which makes this system an excellent case for ionization diagnostics. From the non-detection of Si IV we get the 3σ limit $\log N(\mathrm{Si\,IV}) < 11.3$ cm^{-2}; from the non-detection of N III λ989

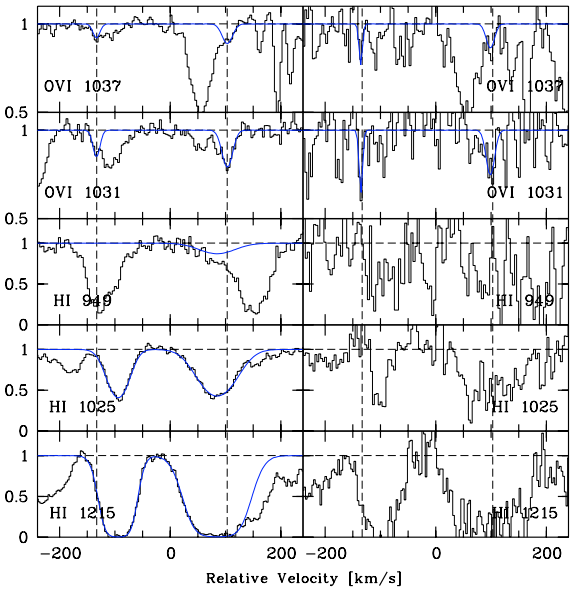

Fig. 10. Class II systems in RX J0911.4+0551. Panels and symbols as for Fig. 3, but for $z = 2.623886$ and $z = 2.626749$.

we get the 3σ limit $\log N(\mathrm{N\,III}) < 12.4$ cm^{-2}; and from non-detection of N V we get the 3σ limit $\log N(\mathrm{N\,V}) < 12.0$ cm^{-2}.

In B there is absorption at the expected position of O VI but a 2-component fit here proved less reliable due to the lower S/N. We fitted a 1-component profile and obtained the same value within errors as the total O VI in A. The same procedure was applied to C IV. Therefore, the b-values displayed in Table 3 have no physical meaning if this system indeed is composed of 2 velocity components along LOS B too. The H I was too difficult to constrain in B again because of the high noise level.

$z = 2.623886$ and $z = 2.626749$, $S = 0.6$ kpc, Class II systems in RX J0911.4+0551, see Fig. 10 For these two systems, the predicted position of C IV lies within spectral gaps. We do not detect Si IV, and C III, N V and S VI are blended. From non-detection of Si IV we get the 3σ limit $\log N(\mathrm{Si\,IV}) < 11.3$ cm^{-2}. This is not proof against the identifications (neither of these ions is expected in an O VI phase if the gas is photoionized), but it makes the O VI identification less reliable. We note that H I is not aligned with O VI in either system. Although attempting Voigt profile fits in B may seem daring, they again show that O VI cannot differ significantly from one LOS to the other in neither system.

$z = 2.631480$ through $z = 2.634119$, $S = 0.5$ kpc, Class I system in RX J0911.4+0551, see Fig. 11 This is a LLS with a total neutral hydrogen column density in A of $\log N(\mathrm{H\,I}) = 16.56$ cm^{-2}. This value comes from the unsaturated H I λ918 line, for which we fit 4 velocity components. This system was evident already in the discovery spectrum of Bade et al. (1997) and lies $v = 11\,000$ km s^{-1} from the QSO systemic redshift, so we regard it as intervening. Although C IV falls in the gap, the Si IV is evident and rich in structure. Also, lower ionization species are detected (not shown in the figure) such as C II, N III, and Si III.

We seem to have clearly detected S VI aligned with the strongest Si IV component. There have been few reports of intervening S VI in the literature. Savage et al. (2005) have studied a system at $z = 0.2$ with $N_{\mathrm{H\,I}} \approx 15.0$ cm^{-2}, that shows O VI, Ne VIII, S VI, and a wide range of low-ionization species. They have shown that photoionization explains the low-ionization species, including S VI, but is not able to reproduce the O VI.

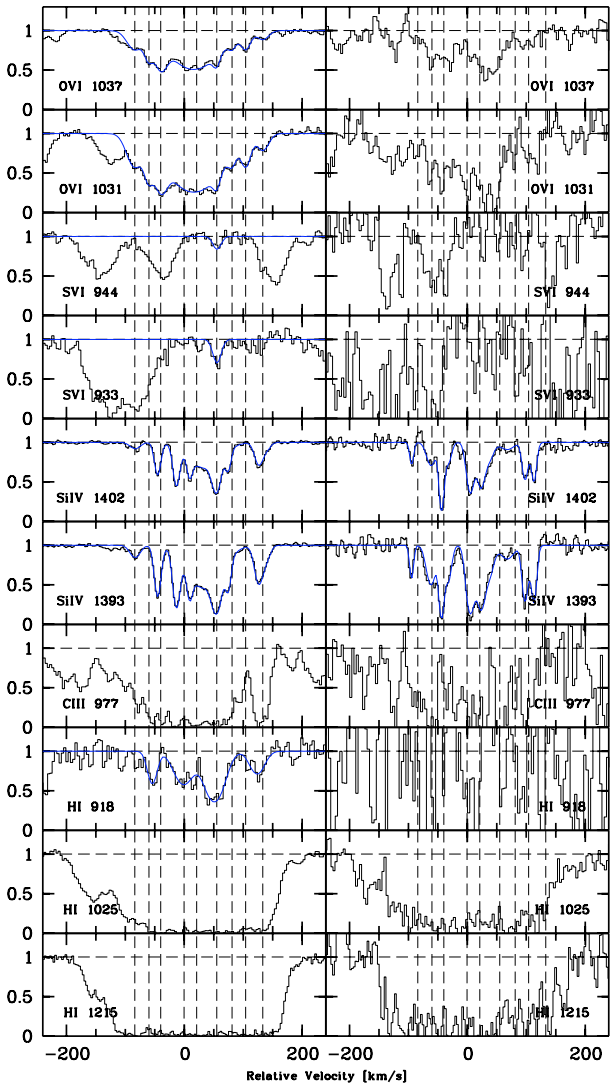

Fig. 11. Class I system in RX J0911.4+0551. Panels and symbols as for Fig. 3, but for $z = 2.631480$, $z = 2.631768$, $z = 2.632020$, $z = 2.632495$, $z = 2.632770$, $z = 2.633161$, $z = 2.633486$, $z = 2.633766$, and $z = 2.634119$.

We have fitted 9 velocity components in each spectrum. In A, we note the disparity between the line centroids of O VI and Si IV. However, the velocities of the Si IV and H I are more similar (although due to higher thermal broadening we do not resolve as many lines in H I as in Si IV).

The much lower S/N at O VI in spectrum B prevents a reasonable fit. To compare both LOS we first calculated the O VI column density in A using both line profile fitting and the Apparent Optical Depth Method (AODM). The total O VI column density from the fits was $\log N(\mathrm{O\,VI}) = 14.76 \pm 0.07$ cm^{-2}, while from the AODM we obtained $\log N(\mathrm{O\,VI}) = 14.74 \pm 0.01$ cm^{-2} (integrating in the range $[-150, 160]$ km s^{-1}, and averaging the λ1031 and λ1037 values). The good match between these independent estimates indicates that the lines are not heavily saturated. We repeated the pixel sum within the same velocity interval along LOS B and obtained $\log N(\mathrm{O\,VI}) = 14.66 \pm 0.07$ cm^{-2}, indicating that the differences in O VI column density between A and B are negligible. Differences in

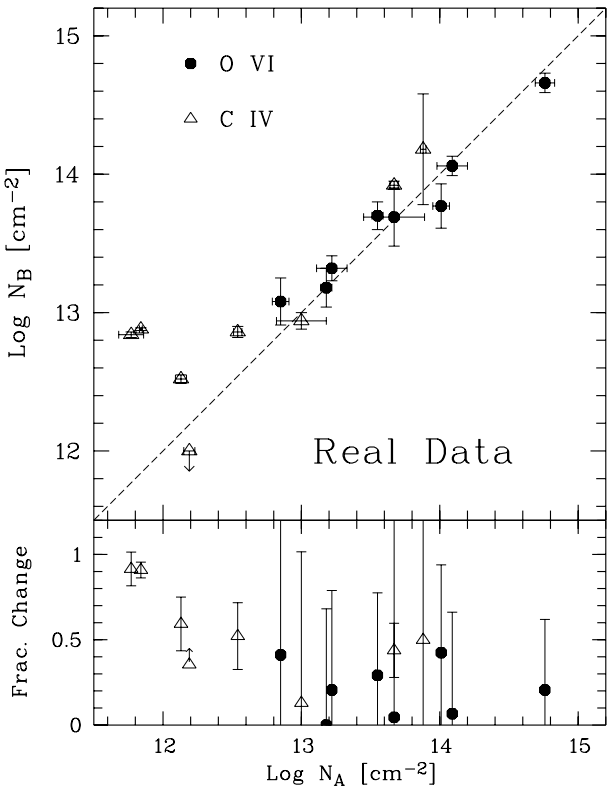

Fig. 12. Comparison of column densities between the A and B lines of sight (upper panel), and fractional change between A and B, $|N_A - N_B|/\max(N_A, N_B)$ for O VI and C IV in O VI systems. For clarity, the two upper limits on $N(\mathrm{O\,VI})_B$ have not been displayed. The associated systems have not been included.

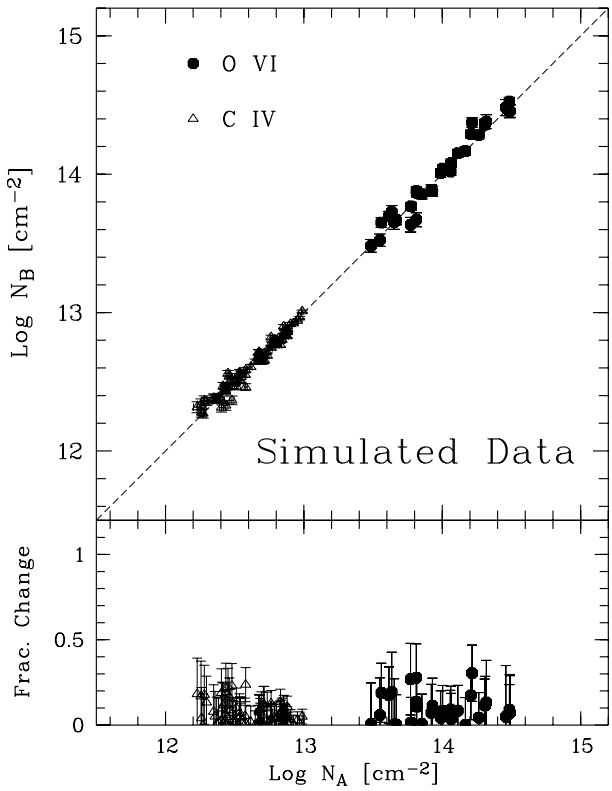

Fig. 13. Same as in Fig. 12 but for simulated data. Column densities were recovered automatically from a sample of synthetic O VI and C IV lines with random redshifts and column densities and same S/N and blending levels as in the real data (see text for more details). The simulated column densities are identical in the two lines of sight.

kinematical structure between A and B are also much more evident in Si IV than in O VI.

4. Comparisons across the lines-of-sight

4.1. Column densities

Figure 12 shows a comparison between column densities in A and B according to the values listed in Table 3 and excluding the associated systems. Column densities are summed over velocity components when the other LOS has a value labeled with footnote *b* in the table. It can be seen that the O VI systems do not present significant LOS differences (the 2 upper limits – not displayed in the figure – are consistent with no differences). In contrast 6 out of the 8 C IV systems significantly deviate from the straight line of unity-slope (for the LLS at $z = 2.63$ note that we have used Si IV as a proxy for C IV). This is also evident in the fractional changes (lower panel of the figure) where we see that while the data is consistent with a null change in O VI, 6 out of the 8 C IV systems in which we detect O VI show, on the contrary, significant changes of up to 90%. We have to keep in mind that C IV column densities are measured redwards of the forest and at higher S/N than O VI column densities. We estimate that errors in O VI column densities in the noisier B spectrum prevent us to assess possible changes in O VI of ≈40% or lower.

In order to assess the impact of blending and S/N in the O VI region of the spectrum compared with the C IV region, we have run Monte Carlo simulations. Specifically, we synthesize O VI and C IV lines with random redshifts and column densities (within the observed ranges) and merge them with the real data. Two samples of spectra are created; in the first, the column densities are identical in the two lines of sight, in the second we introduce a column density difference of 0.5 dex (fractional change of ∼0.7). In the latter sample, the higher column density may be present in either LOS A or B. For 300 realizations, we then attempt to recover the synthesized lines by using the same search and fitting techniques as for the real data (the only exception being that line widths are kept fixed at the simulated values, which makes error bars on the column densities smaller than for the real lines). For the sample with equal column densities in the two LOS, Fig. 13 shows the recovered column densities in the same format as in Fig. 12. We find that the recovered $N_{\mathrm{O\,VI}}$ and $N_{\mathrm{C\,IV}}$ values in the synthesized systems have fractional changes <0.2 for 90% and 95% of the cases, respectively, i.e., consistent with equal column densities in the two LOS. In the sample for which the column densities differ by 0.5 dex in the two LOS (Fig. 14) the recovered fractional change is on average 0.70 for O VI and 0.65 for C IV, with a rather small dispersion of ≈0.10 for both samples. The fact that column densities are recovered with high statistical significance for both mock samples indicates that differences in S/N or effects of blending in the Lyα forest should not bias our results toward enhanced coherence in O VI compared with C IV.

It is also interesting to note that two of the three "Class I" systems, regarded as more certain, show respectively low and high fractional changes for O VI and C IV. In summary, we conclude that we have detected an excess of transverse structure in the C IV profiles when compared with O VI, a fact that lead us to conclude that a significant fraction of C IV possibly does not trace the same volume as the O VI-bearing gas.

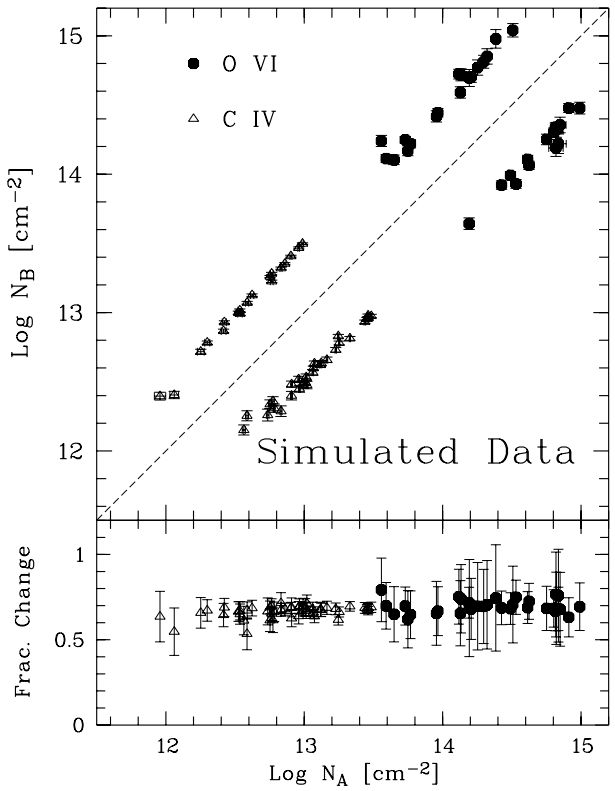

Fig. 14. Same as in Fig. 13 but the simulated column densities differ by 0.5 dex (fractional change of ∼0.7), with the higher column density present in either LOS A or B.

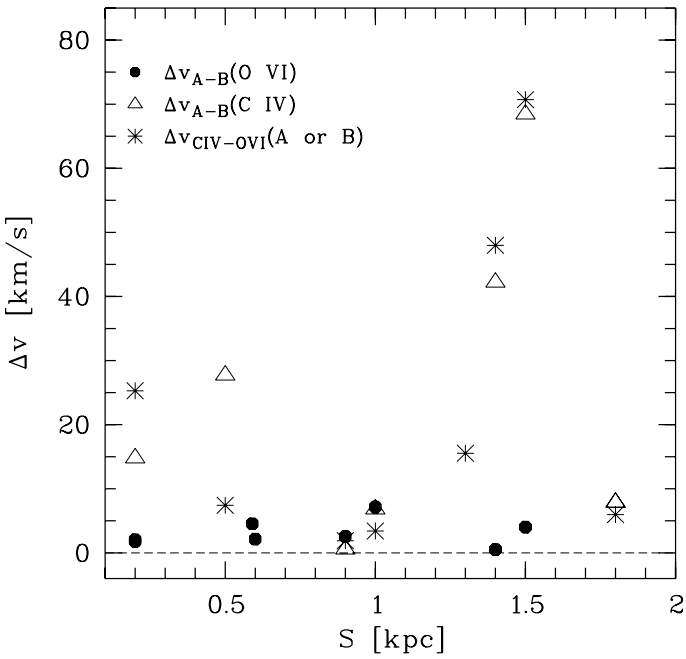

Fig. 15. Velocity shear Δv between LOS A and LOS B (filled circles for O VI and open triangles for C IV) and between C IV and O VI along LOS A or LOS B (asterisks) as a function of proper LOS separation, S. Errors in Δv are at most ∼3–5 km s^{-1} (from line fitting). The associated systems have not been included.

At first glance, this result seems in contradiction with previous studies of C IV in lensed QSOs where coherence has been found on scales considerably larger than probed here. For example, in the compilation of Ellison et al. (2004), there is only a difference of ∼30% for LOS separated by a few kpc. The fractional column density difference rises to 50% for separations ∼100 kpc, whereas here we find 90% variation on a 1 kpc scale. This apparent discrepancy can be explained by the selection criteria of absorbers for our study. Our fundamental pre-requisite is that an absorber exhibit O VI, whereas the majority of C IV absorbers in previous samples do not show this species. If we consider C IV-only (as opposed to O VI+C IV) systems in our 2 lensed QSOs, we see a much higher level of coherence, with fractional variations ∼10% (Lopez et al., in preparation).

A second implication concerns the coherence length of the absorbers, i.e., the scale at which significant changes in column density appear. Systems with $N_{\rm O\,VI} \gtrsim 10^{12.9}$ cm^{-2} at $z = 2.5$ must be much larger than the LOS separation scales of ≈kpc, given their lack of structure across the LOS. Furthermore, in absorbers which exhibit both C IV and O VI, the coherence length of the former must be smaller than the latter. Since potential O VI systems occurring in just one LOS are likely not missing from our sample – given the agreement of our O VI number statistics with previous estimates –, this last conclusion seems generic to all O VI+C IV absorbers at high redshift.

It is interesting to compare our transverse LOS sizes with those inferred from the ionization models of Simcoe et al. (2006). For ∼30 absorbers with multiple transitions, Simcoe et al. (2006) derived metallicities and cloud sizes. They concluded that the majority of O VI absorbers have high metallicities (up to $\sim 1/3\ Z_\odot$) and small sizes (<1 kpc) which inhabit volumes of 100–200 kpc around high redshift, star-forming galaxies. Only around 25% of the O VI absorbers modeled by Simcoe et al. (2006) had sizes larger than 1 kpc. However, Simcoe et al. (2006) also point out that cross-section arguments indicate much larger dimensions; combining this with the small cloud sizes yielded by their ionization models led them to suggest a filamentary or sheet-like geometry. In contrast to the mostly sub-kpc sizes inferred by Simcoe et al. (2006), we find that all O VI absorbers in our lensed QSOs (with LOS separations ∼1 kpc) appear in both LOS and with very similar column densities. This either indicates O VI clouds with sizes >1 kpc or a high filling factor of small clouds. The latter scenario was proposed by Ellison et al. (2004) to explain the coherence between Mg II systems toward the triply imaged QSO APM08279+5255. Although a Mg II absorber observed in one LOS was frequently observed in the others, the difference in fractional column densities could be large, and the line profiles were often very different. However, this does not seem to be the case for the O VI absorbers. In the cases where the S/N is high enough that good Voigt profiles could be obtained (e.g. Figs. 7 and 9), the velocity profiles are very well-matched. We therefore conclude that the O VI clouds included in this sample have sizes larger than ∼1 kpc.

4.2. Velocity

Figure 15 shows the velocity shear between LOS A and B as traced by C IV and O VI. We also show the velocity differences between C IV and O VI along LOS A or LOS B as a function of LOS separation. H I was not included in the figure because line centroids are not well constrained. The small number of systems in B for which we were able to get a Voigt profile precludes a full quantitative analysis on velocity shifts. Nevertheless, we can point out the following facts: (1) there is a clear offset between O VI and C IV (or Si IV) velocity components along LOS A in the three systems with the highest H I column densities, $N_{\rm H\,I} > 10^{15}$ cm^{-2}: the $z = 2.086682$ absorber

and the two LLSs. These systems also show differences in C IV or Si IV between LOS A and B ($\Delta v_{\rm A-B}$(C IV)), apparently independent of LOS separation. Since LLSs are believed to be bound to collapsed structures, $\Delta v_{\rm A-B}$(C IV) $\neq 0$ (though not necessarily $\Delta v_{\rm C\,IV-O\,VI}(A)\neq 0$) are expected on kpc scales. (2) The 2 systems at $z = 2.052440$ and $z = 2.437271$ (both probed at large separations) show the largest offsets both in C IV between A and B, and between C IV and O VI in one of the LOS. Interestingly, these are the 2 systems in our sample where H I appears "detached" from the metals. These systems are considered in more detail below.

Altogether, velocity offsets reinforce the notion that the O VI and C IV in our sample occupy (at least partially) different gas volumes.

4.3. Line widths

Considering only the "A" spectra (with better S/N), in all 5 intervening systems where b-values are relatively well constrained because they have single velocity components, we find $b_{\rm O\,VI} < 12$ km s^{-1}, implying temperatures $T < 1.4 \times 10^5$ K. At this temperature and range of $N_{\rm H\,I}$, models of collisionally ionized plasma (e.g., Prochaska et al. 2004) predict much less O VI than what we observe here. This indicates that photoionization is likely to be the dominant process, as has been found for the majority of known O VI systems at high redshift (Bergeron et al. 2002; Carswell et al. 2002).

An important exception may be the LLS at $z = 2.633$, some of whose velocity components have b-values ≈40–50 km s^{-1}. These may be artifacts due to the more complex kinematics of this system (we note some degree of blending with H I interlopers), or a real hint of collisional ionization.

Regarding line-broadening mechanisms, previous samples contain a mix of systems with lines dominated by either turbulence or thermal broadening. Again, considering only the LOS A in our sample, out of the 5 intervening systems where b-values are well constrained, 4 show clear thermal broadening, with b(O VI) $\approx \frac{1}{4} b$(H I) within errors ($z = 2.086682$, $z = 2.158112$, $z = 2.623886$, and $z = 2.626749$), and one ($z = 2.437271$) has anomalous b-values. The system at $z = 2.517045$ has b-values that suggest a mild contribution from turbulent-motions, but the velocity components are not resolved, so b is less reliable there. Therefore, none of the systems along LOS A seems to be turbulence-dominated.

Finally, if we compare LOS, we note that 4 out of the 5 systems where $b_{\rm O\,VI}$ could be measured in both spectra present no transverse variations in the line widths. In contrast, the (few) $b_{\rm C\,IV}$-values measured are more disparate between LOS. This is another hint that the C IV and O VI absorbing gas may occupy different locations.

4.4. Comparison with O VI in the Galaxy

We can compare the results of this Section with O VI studies in the Galaxy. The distribution of O VI in the Halo is shown to be clumpy, with fractional changes well in excess of what we observe at high redshift (Savage et al. 2003); homogeneous O VI is only shown by very small scales (a few pc; Lehner & Howk 2004). But this is not the only quantitative difference with our high-redshift observations. First, Savage et al. (2003) have indicated that C IV might be kinematically less complex and less disturbed than O VI in the Halo; secondly, they find N(C IV)/N(O VI) = 0.6 ± 0.1 (average over ∼100 LOS), in contrast to all high-redshift systems studied in this paper, where we find N(C IV)/N(O VI) ≈ 0.1 (excluding the LLS). Therefore, the systems probed by these double LOS must be of different nature than the Galactic ones, a fact which should not surprise given the different physics involved in each of them, warm-hot photoionized and hot collisionally-ionized gas, respectively.

5. Photoionization models and a case study

For the reasons outlined in Sect. 4.3, in what follows we consider the O VI gas to be photoionized. Photoionization balance is governed by the ionization parameter, U, the ratio of hydrogen ionizing photon density to total hydrogen density, $n_{\rm H}$. In principle, we could constrain U by (a) assuming an ionizing background spectrum, and (b) varying the gas metallicity to match observed $N_{\rm O\,VI}$ and $N_{\rm C\,IV}$ with model. However, this approach still requires assumption of the [C/O] ratio and that the two measured species arise in the same volume. In addition, softer spectra are degenerate with more diffuse (larger) clouds. This degeneracy can be broken with input from hydrodynamical simulations which correlate $n_{\rm H}$ with $N_{\rm H\,I}$ (with a mild dependence on temperature) at least in the low-density regime and when hydrostatic equilibrium applies (e.g., Schaye 2001). However, in general, the lack of enough ionization stages of the same element makes detailed photoionization modeling uncertain.

One of the O VI systems in our sample, at $z = 2.5170$, is well suited for testing photoionization because both C IV and C III are present, so no assumptions on relative abundances of different elements need be made. In addition, $N_{\rm H\,I}$ is relatively well constrained by nonsaturated Lyγ and Lyϵ . Therefore, we can use H I, C III and C IV as "anchors" for photoionization modeling and investigate whether O VI can be reproduced by the models.

5.1. A single-phase model

We start by asking whether photoionized gas can simultaneously host C III, C IV, and O VI. To test this possibility we first need to re-fit the data with tied velocities. The first column in Table 4 lists the observed column densities for a best-fit redshift of $z = 2.517032$. Note that these differ only slightly from those ones in Table 3. Assuming C III and C IV coexist in the same volume, we build a grid of photoionization models using the CLOUDY package (Ferland et al. 1993), with the geometry approximated by a parallel-slab geometry. The ionizing agent is described by the Haardt & Madau (1996) spectrum of the UV background (UVB) at $z = 2.5$ with normalization $\log J_{912} = -21.5$. The spectrum includes contributions from QSOs and AGNs only, whose spectra are described by power laws $F \propto \nu^{-\alpha}$ with spectral index $\alpha = 1.8$; inclusion of star-forming galaxies appears to have little effect on the two carbon species treated here but may have an effect on O VI (see Fig. 3 in Simcoe et al. 2004, and Sect. 5.4 below). Solar abundances are taken from Grevesse & Sauval (1998), except for oxygen which is taken from Allende Prieto et al. (2001).

Figure 16 shows model column densities for C III and C IV, and (assuming solar [C/N,O]) also for N V, and O VI, as a function of radial size S_r. S_r is proportional to U through fixed J_{912} and $N_{\rm H\,I}$. The C III/C IV ratio determines $U = 10^{-0.8}$, which for the assumed value of J_{912} corresponds to $S_r = 200$ kpc (note that these numbers appy to a single cloud in this system). Having determined U, the carbon abundance can be varied to match the observed C III and C IV column densities. The best match is found for [C/H] = −2.20. This is somewhat over the median but within the spread of Lyα forest metallicities around [C/H] = −2.8

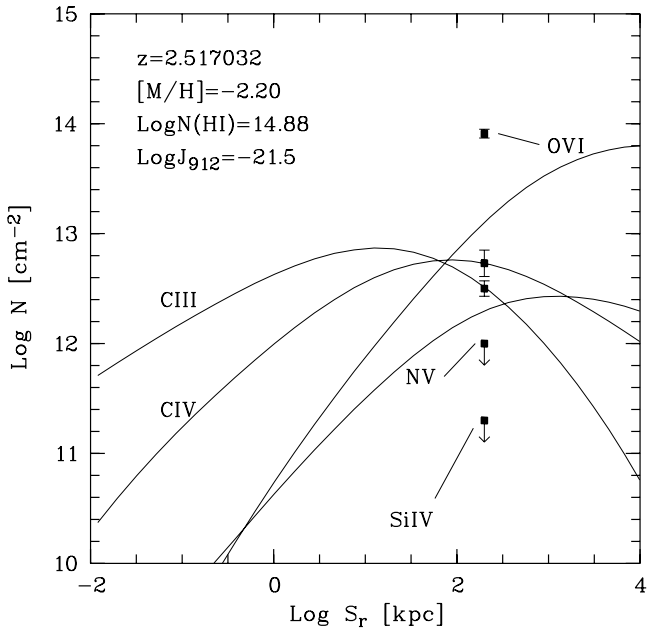

Fig. 16. Single-phase model for O VI system at $z = 2.517032$. Curves are theoretical estimates of column densities as a function of cloud radial dimension S_r for each of the relevant species (labeled on top or below the curves). The model assumes a metallicity [M/H] = −2.20 and solar relative abundances. The Si IV curve lies below the y-axis range. Observed values and their errors all are displayed at the x-axis position that matches C III and C IV.

found by Simcoe et al. (2004) also from photoionization arguments. However, it can be seen that O VI is not reproduced by the model unless oxygen is overabundant with respect to carbon.

With the assumed UVB intensity, the above conditions correspond to a gas density $n_{\rm H} = 10^{-4.1}$ cm^{-3}. The $n_{\rm H}$-$N_{\rm H\,I}$relation yields $n_{\rm H} \lesssim 10^{-3.8}$ cm^{-3} (value assumes a kinetic temperature $T \lesssim 1.0 \times 10^5$ K from the newly-fitted $b_{\rm C\,IV} = 12.0$ km s^{-1}). The CLOUDY solution would match this independent value for a factor of 2 larger clouds, a factor of 2 more intense UVB, or a combination of both.

5.2. A multi-phase model

Assuming homogeneity, it is difficult to think of such large clouds hosting C III-C IV gas, and yet showing transverse structure on kpc scales, as observed in Fig. 12. An overestimate of the size due to an incorrect UVB normalization can be ruled out; uncertainties inherent to this number do exist, but these do not reach two orders of magnitude. A more plausible situation might be that C IV arises in two distinct gas phases, which in turn would explain the offsets observed between C IV and O VI, since the absorption would occur in different volumes[2].

We investigated photoionization models composed of the following two media: a low-ionization phase in which most of the observed C III but only a fraction of the total C IV are present; and a high-ionization phase in which C IV and most of the O VI occurs. Using the simplest approach, H I is distributed so as to keep the same C IV/H I ratio in each media. As for the C IV (and H I) fraction, very unbalanced fractions result in conditions that either approximate to the single-phase model described above or produce unrealistic parameters (sizes of several Mpc at [M/H] = −1 to reproduce O VI-only clouds). Therefore, a "50–50" distribution of the observed C IV appears reasonably representative of the possible variety of cases. Running a new grid of CLOUDY models this time using the modified column densities but the same approach to find U and Z, we determined conditions for both phases independently.

[2] Note that we refer to phases of photoionized gas. As we have argued in Sect. 4.3, we do not find evidence of collisionally ionized gas.

Table 4. Two-phase photoionization model for cloud at $z = 2.517032$.

	Observed	Model	
		Low	High
[C/H]		−2.20	≲−2.10
log U		−1.15	−0.65
log n [cm^{-3}]		−3.75	−4.3
Size [kpc]		20	≲250
[C/O]		0[a]	≈−0.8
[C/N]		...	≳0.2
log N(H I)	14.88	14.58	14.58
log N(C III)	12.50	12.50	≈12.00
log N(C IV)	12.73	12.43	12.43
log N(O VI)	13.92	12.21	13.91
log N(N V)	<12.00	11.60	≲12.00

[a] Assumed.

The results for the (newly-fitted) $z = 2.517032$ system are displayed in Table 4. Getting parameters for the low-ionization phase is straightforward because we match the C IV/C III ratio with the observations without assumptions on relative abundances, as in the single-phase model. This results in a cloud of radial size $S_r = 20$ kpc at [C/H] = −2.20. N(O VI) is 50 times lower than in the high-ionization phase (assuming solar [C/O] – we lack of lower ionization stages of oxygen to constrain [O/H] in this phase), too low to be detected in our data and even for overabundant oxygen it would not be detectable. To model the high-ionization phase a [C/O] ratio has to be assumed since we require that C III does not contribute significantly to the observed value. That ratio is constrained imposing that the radial size be smaller than the maximum size allowed by the H I line width, if it were purely Hubble broadening, or $S_r < 250$ kpc for this particular system. To match the data, [M/H] = −2.10 and [C/O] = −0.8 is required (we discuss this further in the next sections). In addition, our limit on N V requires [C/N] ≳ 0.2 dex (in the low-ionization phase this ratio is also consistent with the limit for N III – see 3.4.).

5.3. Characteristic sizes along the lines of sight

The two-phase model explains simultaneously the observed column density differences in C IV, the velocity shifts between C IV and O VI and the homogeneity of O VI on kpc scales. In fact, $S_r \approx 20$ kpc sizes, if also representative of transverse dimensions, perfectly produce fractional changes in C IV of the order of what we observe here, as demonstrated by size estimates by statistical means from observed fractional changes in C IV on kpc scales (Rauch et al. 2001). As for the high-ionization phase, O VI clouds that extend over a few hundred kpc are expected to produce featureless absorption on the small scales probed with the present data, and, also fitting well to our model, studies of wider QSO pairs have found no correlation of strong C IV systems over ∼300 kpc scales (Becker et al. 2004).

Our "50–50" model is also consistent with the good match between C IV and C III line profiles in all systems where C III is detected (the 2 LLSs, and $z = 2.516$ systems); those cases show that the fraction of C IV in the low-ionization phase cannot be arbitrarily low.

According to our model, if one LOS happens to pass through the two phases while the other LOS does so only through the more extended one, then column density differences of up to 0.3 dex should arise in C IV, C III, *and* H I, while almost the same O VI should be measured along both LOS, a situation that is effectively observed in our sample. Regarding H I, although no firm constraints could be made on column densities, there are some indications of variations of this level in the systems at $z = 2.158112$, and at $z = 2.200800$.

Finally, note that we have imposed homogeneous C IV/H I ratios, so our model explains C IV gradients across the LOS as a consequence of the smaller size of low-ionization phase only, not because of inhomogeneous ionization conditions (within this phase). On the other hand, homogeneous ionization in the extended O VI-phase is supported by the similar line widths observed in LOS A and B. Being thermally-dominated, these similar widths imply the absence of significant temperature gradients, and thus ionization must be homogeneous (at least on the kpc scale and with local ionizing sources being unimportant).

5.4. Uncertainties

The results from previous section suffer from some model and measurement uncertainties.

The first question one may raise is whether the O VI systems are really photoionized. In Sect. 4.3 we have argued that O VI line widths of the general population in our sample suggest photoionized gas. In particular for the $z = 2.517032$ system, although its O VI Doppler value is not very well constrained and does not rule out collisional ionization (this particular measurement is subject to systematics anyway due to the unresolved velocity components), we note that both the presence of C III and the narrow C IV profile hint at photoionized gas (see Prochaska et al. 2004).

A second concern is what effect errors in the continuum can have on the CLOUDY parameters, specially given the limited S/N of our data in this part of the forest. To explore this we recomputed column densities for the $z = 2.517032$ system using flux levels that were displaced artificially by 1σ. The new column densities differ by ∼0.08 dex. The C III/C IV ratio is therefore determined with an uncertainty of at most ∼0.16 dex, which translates into a ∼0.20 dex uncertainty in $\log U$. This means that a wide range of possible radial sizes, $S_r \sim 100{-}500$ kpc for the high-ionization and $S_r \sim 10{-}80$ kpc for the low-ionization phase, are consistent with the data (of course this range assumes that J_{912} is accurate to this limit or better). Therefore, although the derived sizes are quite sensitive to changes in column density, departures from the 50–50 model still result in two size ranges that differ by one order of magnitude.

We then consider the shape and normalization of the UVB. As mentioned before, inclusion of star-forming galaxies (Simcoe et al. 2004) does not affect the region encompassing the C III and C IV ionizing thresholds, but may lower the UVB at the He II edge by ∼0.3 dex. This means that radial sizes (derived from the C III/C IV ratio) remain unaffected, but our result on the C/O ratio may be affected at this level. Secondly, the UVB models contain also uncertainties in the spectral index of the quasar spectra (assumed to be pure power laws). The UVB hardness affects C IV and O VI differentially (Schaye et al. 2003), thus directly affecting our results on the C/O ratio. For instance, a spectral index of $\alpha = 1.5$ (instead of the assumed $\alpha = 1.8$) favors a higher prediction of O VI, and thus a lower C/O by ≈0.4 dex. Finally, the UVB normalization has been constrained with independent methods (statistics of metal species and proximity effect) leading to similar results, and is therefore subject to less important uncertainties.

In conclusion, besides the fact that this is just a case study and may not be widely applicable to absorbers in general, the main caveat of our model seems to be the shape of the UVB, affecting more the derived [C/O] than the sizes.

6. The source of metals

6.1. Relative abundances

Regardless of cloud size, important inferences on relative abundances can be made. In the single-phase model depicted in Fig. 16 we see that O VI and C IV are not reproduced simultaneously unless $[C/O] \approx -0.7$, and a similar situation is found for the two-phase model (but let us emphasize that the predicted [C/O] abundance is affected by the shape of the UVB: a harder [flatter] spectrum, say with $\alpha = 1.5$, would yield $[C/O] \approx -0.4$ only). As for nitrogen, N V should be detected according to our CLOUDY models but it is not, implying $[C/N] \gtrsim 0.2$.

Such abundances may conform to gas that has been enriched recently before the absorption occurred – in contrast to the yields of an early pre-enrichment. The present abundance pattern is similar to direct measurements of C/H and O/H in a few damped Lyα systems (DLA) at similar metallicity levels (e.g., D'Odorico & Molaro 2004). Furthermore, low [N/O] is found in a fraction of low-metallicity DLA, an abundance ratio that has been interpreted as an indicator of recent chemical enrichment (e.g., Pettini et al. 2002; Prochaska et al. 2002).

Our result on [C/O] is also to be compared with measurements of carbon and oxygen in Galactic metal-poor stars. For example, Akerman et al. (2004) have studied the metallicity dependence of [C/O] and confirmed the drop of [C/O] to −0.5 at $[O/H] \approx -1$ ($[C/O] = -0.7$ if non-LTE corrections are considered, see Fabbian et al. 2005). This is roughly the regime we are probing in the O VI system studied in Sect. 5.2. The absorbing gas would be enriched by a first generation of massive stars, just as predicted by Galactic chemical evolution models after completion of the first Gyr of the Halo formation.

Alternatively, the observed gas may be chemically young but have been released to the IGM a long time before the absorption occurred (say, over 2 Gyr before, $z >\sim 6$). Though plausible, this scenario requires another ingredient, namely that the gas that was further processed to reach higher C/O in that time has not reached yet the physical volume probed by the $z = 2$ observations.

It therefore seems that one viable way to reproduce the data on O VI, N V, and C IV via photoionization is with CNO abundances from late rather than early injection of metals. An extended phase of such enriched gas might be in broad line with $[C/Si] \approx -0.8$ measured in the high-z IGM and in similar absorption systems but with a different technique (Aguirre et al. 2004).

6.2. O VI outflows?

The systems at $z = 2.437271$ and $z = 2.052440$ are perhaps good examples of the two-phase scenario and deserve further analysis. Besides their particular velocity offsets (between C IV-O VI and H I along LOS A, and between LOS A and B in C IV – see Fig. 8) these systems also have the highest $N(\mathrm{O\,VI})/N(\mathrm{H\,I})$ ratios in the sample, 1.25 and 1.6, respectively, so both must be highly ionized. Systems with these $N(\mathrm{O\,VI})/N(\mathrm{H\,I})$ ratios are

uncommon but have been reported both at high (Reimers et al. 2001; Bergeron & Herbert-Fort 2006) and low redshift (Tripp et al. 2000).

The observed velocity offsets agree well with the multi-phase model, with a fraction of C IV in a low-ionization phase that is kinematically detached from a more extended O VI phase. In the $z = 2.437271$ system along LOS B, the fraction of C IV that would arise in the high-ionization phase (expected at the position of the dashed line) is lost in the noise. In addition, the H I profile in B suggests a slightly lower column density than in A, just as expected (Sect. 5.3) from our two-phase model. A similar situation is found for the $z = 2.052440$ system.

Repeating the CLOUDY simulations for these systems is more uncertain because C III is not available, and thus U can only be constrained if a value for [C/O] is assumed. Taking the $z = 2.437271$ system along LOS A as an example, the 50–50-C IV distribution yields a high-ionization phase with $S_r = 50$ kpc for [C,O/H] = −0.75 (i.e., assuming solar [C/O]).

This C IV gas, perturbed on kpc scales (Rauch et al. 2001) and two orders of magnitude more metal-rich than the average Lyα forest (Simcoe et al. 2004), is highly suggestive of gas close to overdense regions with a high star-formation rate. Moreover, the transverse velocity offsets and column density differences of C IV and H I also suggest possible gas outflows with ejection velocities of a few hundred km s^{-1}, due to violent dynamical processes driven by supernovae explosions.

Highly ionized, metal-rich O VI systems detected toward single QSOs have been interpreted as gas outflows before (e.g., Aracil et al. 2004; Simcoe et al. 2006; Fox et al. 2007). The tens-of-km s^{-1} shifts we detect here in C IV might be a signature of such possible effects across the LOS (although we stress that these two systems have O VI line widths consistent with photoionization and $N_{\rm H\,I}$ much lower than those probed by the sample of Simcoe et al. 2006). The observed profiles could alternatively be explained by gas associated with high-redshift disks or extended halos, but recall from Sect. 4.4 that such halos would have to be quite different in nature from the local one.

Another interesting point is that only C IV shows disturbance on these scales, not O VI. One possible interpretation is that this kind of outflows do not transport highly ionized gas. Note that this picture does not depend on the lower significance of the O VI detection in the $z = 2.437271$ systems along LOS B, since O VI aligned with C IV is discarded by the data (assuming same O VI/C IV ratio as in A). O VI-bearing gas outflow would require detection of O VI aligned with C IV in B too, which is definitely not the case.

6.3. Distribution of metals

Correlations between galaxies and metal systems at $z = 2-3$ have recently shown that O VI is always found at distances of up to a few hundred kpc from an observed galaxy (Adelberger et al. 2005; Simcoe et al. 2006). Our constraints on characteristic absorber sizes and relative abundances from photoionization models *and* on sizes and kinematic properties from observed transverse differences all fit well into a scenario of galaxy feedback. The extended O VI-phase we detect here, though quite homogeneous on kpc scales, apparently is dominated by metals that have been put in place only recently by type II SNe, in contrast to – or on top of – an early wide spread by Pop III stars.

Other observations (e.g., Adelberger et al. 2005) have indicated that gas *is* able to escape galaxies and pollute the IGM up to large distances, and this process may result in an inhomogeneous metal enrichment as suggested by simulations (e.g., Theuns et al. 2002; Aguirre & Schaye 2005). We may have detected a new signature of this process in the disturbed C IV that is associated with the O VI systems. However, the dissociation between C IV and O VI observed here (both along and across the LOS) is somewhat uncomfortable within that simple picture and may also indicate that the possible outflows required to transport the metals have different time scales for the different species (and thus ionization stages), with O VI having been "in place" well before C IV. On the other hand, we do not see the signature of shock-heated gas; if O VI systems like the one at $z = 2.437271$ are representative of such violent processes, then why does the gas appear predominantly photoionized? What fraction of the observed O VI indeed comes from galaxy feedback – in contrast to arising in pre-enriched gas – remains to be investigated for example with similar observations of binary QSOs to probe larger scales.

7. Summary and conclusions

We have searched for O VI systems in spatially-resolved high-resolution spectra of two lensed QSOs. Applying a well-defined searching method independently to each spectrum we have detected O VI in 10 intervening H I systems. Their redshifts range between $z = 2.010$ and 2.633, and their O VI column densities between $10^{12.9}$ and $10^{13.9}$ cm^{-2}. We have used the information provided by differences and similarities across the lines of sight in the line parameters of various species to extract physical parameters via photoionization models. Given the inhomogeneous character of the data – different S/N ratios and degrees of blending –, we have paid special attention to the observational errors. We have also discussed the uncertainties of the photoionization models. In addition to this analysis, in the Appendix we present 3 associated systems that also show absorption by O VI. Our conclusions for the intervening systems are as follows:

1. Every O VI system detected in one LOS shows O VI also in the adjacent LOS. Since the observed number density of O VI is in agreement with previous studies and since H I interlopers are believed not to show strong variations on kpc-scales, potential O VI systems in only one LOS are likely not missing from our sample.
2. Within uncertainties, $N_{\rm O\,VI}$ shows little structure across the LOS, which probe the gas on transverse scales of 0.2–1.4 h_{70}^{-1} kpc, and the data are consistent with a null fractional change on these scales. Unfortunately, the low S/N in the Lyα forest of the B sightlines does not allow us to probe fractional changes lower than ∼40% and the upper error bars are in some cases consistent with high values. On the other hand, the more certain "Class I" systems all show low fractional changes, thus supporting an O VI coherence length in excess of 1 kpc. The situation for C IV is fully different. Six out of the 8 systems in which we detect C IV show a fractional change in this species that is large (up to 90%) and significant.
3. C IV and O VI systematically show velocity offsets between line centroids while in the case where C III is detected, it seems to follow C IV. There are also significant velocity offsets in C IV between LOS A and LOS B, but none of the O VI systems show such offsets. Doppler widths indicate photoionized gas, and these also do not seem to vary between LOS.
4. The observed properties of species in the 2 LOS support a scenario in which an important fraction of C IV may not reside in the same volume as O VI. This is consistent with

photoionization models that predict clouds with unrealistically large sizes if both ions are taken into account. A two-phase model in which C IV arises both in a low and a high-ionization regime, with characteristic sizes of a few tens and a few hundreds of kpc, respectively, successfully explains the various LOS differences.

5. The observed O VI puts constraints also on abundances, and photoionization requires for these clouds CNO abundances consistent with gas processed in galaxies recently before the absorption epoch. This implies that the absorbing gas is likely dominated by some kind of galactic feedback and/or it occurs not too far away from star-forming regions, although the observed O VI is of a very different nature than in the Galaxy. In particular, the systems at $z = 2.052$ and $z = 2.437$ are consistent with the lines of sight crossing a metal-rich galactic outflow. However, from its kinematics across the LOS, O VI does not seem to be transported in the expelled gas.

Acknowledgements. We have benefitted from conversations with Jacqueline Bergeron, Todd Tripp and Jason X. Prochaska. We are also indebted to the referee, Joop Schaye, for insightful criticisms. The Haardt & Madau (1996) spectrum was kindly provided to us by Francesco Haardt. SL thanks the ESO Scientific Visitor Program for supporting a pleasant stay at ESO Headquarters, where part of this work was done. S.L. was partly supported by the Chilean *Centro de Astrofísica* FONDAP No. 15010003, and by FONDECYT grant N°1060823.

References

Adelberger, K., Steidel, C. C., Shapley, A. E., & Pettini, M. 2003, ApJ, 584, 45
Adelberger, K., Shapley, A. E., Steidel, C. C., et al. 2005, ApJ, 629, 636
Aguirre, A., & Schaye, J. 2005, in Proc. IAU 199 Conf., Probing Galaxies through Quasar Absorption Lines, ed. Williams, Shu, Menard
Aguirre, A., Hernquist, L., Schaye, J., et al. 2001, ApJ, 561, 521
Aguirre, A., Schaye, J., Kim, T.-S., et al. 2004, ApJ, 602, 38
Akerman, C. J., Carigi, L., Nissen, P. E., Pettini, M., & Asplund, M. 2004, A&A, 414, 931
Allende Prieto, C., Lambert, D. L., & Asplund, M. 2001, ApJ, 556, 63
Aracil, B., Petitjean, P., Pichon, C., & Bergeron, J. 2004, A&A, 419, 811
Bade, N., Siebert, J., Lopez, S., Voges, W., & Reimers, D. 1997, A&A, 317, 13
Barlow, T. A., & Sargent, W. L. W. 1997, AJ, 113, 136
Becker, G. D., Sargent, W. L. W., & Rauch, M. 2004, ApJ, 613, 61
Bergeron, J., & Herbert-Fort, S. 2005 [arXiv:astro-ph/0506700]
Bergeron, J., Aracil, B., Petitjean, P., & Pichon, C. 2002, A&A, 396, L11
Bianchi, S., Cristiani, S., & Kim, T.-S. 2001, A&A, 376, 1
Bowen, D. V., Jenkins, E. B., Tripp T. M., Sembach K. R., & Savage, B. D., Proceedings of Astrophysics in the Far Ultraviolet: Five Years of Discovery with FUSE, PASP, ed. Sonneborn, Moos & Andersson [arXiv:astro-ph/0410008]
Burud, I., Courbin, F., Lidman, C., et al. 1998, ApJ, 501, 5
Carswell, B., Schaye, J., & Kim, T.-S. 2002, ApJ, 578, 43
Cowie, L. L., & Songaila, A. 1998, Nature, 394, 44
Danforth, C. W., & Shull, J. M. 2005, ApJ, 624, 555
Danforth, C. W., Shull, J. M., Rosenberg, J. L., & Stocke, J. T. 2005 [arXiv:astro-ph/0508656]
Davé, R., Hellsten, U., Hernquist, L., Katz, N., & Weinberg, D. H. 1998, ApJ, 509, 661
D'Odorico, V., & Molaro, P. 2004, A&A, 415, 879
Ellison, S. L., Songaila, A., Schaye, J., & Pettini, M. 2000, AJ, 120, 1175
Ellison, S. L., Ibata, R., Pettini, M., et al. 2004, A&A, 414, 79
Fabbian, D., Asplund, M., Carlsson, M., & Kiselman, D. 2005 [arXiv:astro-ph/0508063]
Ferland, G. J. 1993, University of Kentucky, Physics Department Internal Report
Fox, A. J., Savage, B. D., & Wakker, B. P. 2006, ApJS, 165, 229
Fox, A. J., Petitjean, P., Ledoux, C., & Srianand, R. 2007 [arXiv:astro-ph/0701392]
Ganguly, R., Sembach, K. R., Tripp, T. M., Savage, B. D., & Wakker, B. P. 2006, ApJ, 645, 868
Grevesse, N., & Sauval, A. J. 1998, Space Sci. Rev., 85, 161
Haardt, F., & Madau, P. 1996, ApJ, 461, 20
Haehnelt, M. G., Steinmetz, M., & Rauch, M. 1996, ApJ, 465, L95
Indebetouw, R., & Shull, J. M. 2004, ApJ, 607, 309
Kneib, J.-P., Cohen, J. G., & Hjorth, J. 2000, ApJ, 544, L35
Lehner, N., & Howk, J. C. 2004, PASP, 116, 895
Levshakov, S., Agafonova, I., Reimers, D., & Baade, R. 2003, A&A, 404, 449
Lidman, C., Courbin, F., Kneib, J.-P., et al. 2000, A&A, 364, L62
Lopez, S., Reimers, D., Rauch, M., Sargent, W. L. W., & Smette, A. 1999, ApJ, 513, 598
Lopez, S., Hagen, H.-J., & Reimers, D. 2000, A&A, 357, 37
Lopez, S., Reimers, D., Gregg, M. D., et al. 2005, ApJ, 626, 767
Petitjean, P., Surdej, J., Smette, A., et al. 1998, A&A, 334, L45
Pettini, M., Ellison, S. L., Bergeron, J., & Petitjean, P. 2002, A&A, 391, 21
Pieri, M. M., Schaye, J., & Aguirre, A. 2006, ApJ, 638, 45
Prochaska, J. X., Henry, R. B. C., O'Meara, J. M., et al. 2002, PASP, 114, 933
Prochaska, J. X., Chen, H.-W., Howk, J. C., Weiner, B. J., & Mulchaey, J. 2004, ApJ, 617, 718
Qian, Y., & Wasserburg, G. 2005, ApJ, 623, 17
Rauch, M., Sargent, W. L. W., & Barlow, T. A. 2001, ApJ, 554, 823
Rauch, M., Becker, G. D., Viel, M., et al. 2005, ApJ, 632, 58
Reimers, D., Baade, R., Hagen, H.-J., & Lopez, S. 2001, A&A, 374, 871
Savage, B. D., Sembach, K. R., Wakker, B. P., et al. 2003, ApJS, 146, 125
Savage, B. D., Lehner, N., Wakker, B. P., Sembach, K. R., & Tripp, T. M. 2005, ApJ, 626, 776
Scannapieco, E., Ferrara, A., & Madau, P. 2002, ApJ, 574, 590
Schaye, J. 2001, ApJ, 559, 507
Schaye, J., Rauch, M., Sargent, W. L. W., & Kim, T.-S. 2000, ApJ, 541, L1
Schaye, J., Aguirre, A., Kim, T.-S., et al. 2003, ApJ, 596, 768
Simcoe, R. A., Sargent, W. L. W., & Rauch, M. 2002, ApJ, 578, 737
Simcoe, R. A., Sargent, W. L. W., & Rauch, M. 2004, ApJ, 606, 92
Simcoe, R. A., Sargent, W. L. W., Rauch, M., & Becker, G. 2006, ApJ, 637, 648
Smette, A., Surdej, J., Shaver, P. A., et al. 1992, ApJ, 389, 39
Smette, A., Robertson, J. G., Shaver, P., et al. 1995, A&AS, 113, 199
Stocke, J. T., Penton, S. V., Danforth, C. W., et al. 2006, ApJ, 641, 217
Telfer, R. C., Zheng, W., Kriss, G. A., & Davidsen, A. F. 2002, ApJ 565, 773
Theuns, T., Viel, M., Kay, S., et al. 2002, ApJ, 578, L5
Tzanavaris, P., & Carswell, R. F. 2003, MNRAS, 340, 937
Tripp, T. M., & Savage, B. D. 2000, ApJ, 542, 42
Tripp, T. M., Savage, B. D., & Jenkins, E. 2000, ApJ, 534, L1

Online Material

Table 3. Intervening O VI systems toward HE1104-1805 A and B, and RX J0911.4+0551 A and B.

	LOS A			LOS B				
Ion	z	log N	b	z	log N	b	Class	QSO
H I	2.010370	14.39(0.01)	41.3(0.9)				II	HE1104-1805
C IV	2.010531	11.84(0.07)	5.5(1.6)	2.010452	12.88(0.01)	7.6(0.3)		
O VI	2.010473	13.39(0.21)	9.8(6.1)		<13.7			
H I				2.052476	13.48(0.02)	24.5(1.6)	II	HE1104-1805
C IV	2.053196	11.77(0.09)	5.2(2.1)	2.052499	12.84(0.02)	8.9(0.5)		
O VI	2.052481	14.01(0.06)	8.3(1.7)	2.052440	13.77(0.16)	7.4(4.5)		
H I	2.086492	>15.11(0.01)	29.9(0.7)				II	HE1104-1805
C IV	2.086522	12.19(0.04)	9.6(1.1)		<12.0			
O VI	2.086682	13.21(0.11)	10.5(3.5)		<13.5			
H I	2.158179	>14.70(0.02)	26.7(0.4)	2.158165	>14.80(0.05)	27.9(0.6)	II	HE1104-1805
C IV	2.158093	12.13(0.04)	10.2(1.4)	2.158087	12.52(0.03)	9.5(1.0)		
O VI	2.158112	13.22(0.11)	4.6(2.9)	2.158139	13.32(0.09)	8.6(2.0)		
H I		16.67(0.12)[a]			17.00(0.08)[a]		II	HE1104-1805
C IV		13.67(0.03)[b]			13.92(0.03)[b]			
O VI	2.200800	13.00(0.20)	4.8(3.3)	2.200822	13.34(0.15)	7.2(3.5)		
O VI	2.201069	13.57(0.08)	16.7(4.4)	2.201088	13.44(0.15)	12.6(5.9)		
H I	2.435220	13.93(0.04)	37.6(2.9)				I	RX J0911.4+0551
H I	2.436189	14.86(0.02)	36.6(1.0)					
H I	2.437021	13.64(0.07)	71.1(5.8)					
C IV	2.437208	12.54(0.03)	13.9(1.2)	2.436724	12.86(0.04)	6.4(1.0)		
O VI	2.437271	13.55(0.04)	10.0(1.0)	2.437265	13.70(0.10)	10.6(3.7)		
H I	2.516735	14.82(0.03)	59.8(2.2)				I	RX J0911.4+0551
C III	2.516871	12.18(0.20)	26.7(0.0)					
C IV	2.516871	12.67(0.14)	26.7(5.2)					
O VI	2.516735	13.62(0.10)	12.8(2.7)					
H I	2.517045	14.88(0.03)	31.9(1.3)					
C III	2.516995	12.50(0.07)	12.7(0.0)		<12.53			
C IV	2.516996	12.73(0.12)	12.7(1.6)	2.516916	12.92(0.06)[b]	17.6(2.6)		
O VI	2.517045	13.91(0.04)	16.7(1.5)	2.516961	14.06(0.07)[b]	22.8(4.2)		
H I	2.624316	13.84(0.77)	27.1(3.5)				II	RX J0911.4+0551
H I	2.624381	14.08(0.44)	23.8(2.1)					
O VI	2.623886	12.85(0.06)	7.7(1.6)	2.623860	13.08(0.17)	1.9(0.9)		
H I	2.626526	14.49(0.01)	44.3(0.7)				II	RX J0911.4+0551
O VI	2.626749	13.18(0.04)	12.4(1.5)	2.626694	13.18(0.14)	9.6(4.7)		
H I	2.631842	15.66(0.07)	10.0(2.3)				I	RX J0911.4+0551
O VI	2.631480	13.66(0.06)	17.3(2.5)					
H I	2.632487	15.98(0.06)	21.6(3.4)					
O VI	2.631768	13.54(0.09)	8.9(1.2)					
O VI	2.632020	13.83(0.05)	12.9(1.1)					
H I	2.633119	16.25(0.04)	21.5(2.4)					
O VI	2.632495	13.91(0.15)	47.3(13.6)					
O VI	2.632770	14.43(0.04)	52.5(4.0)					
H I	2.633998	15.66(0.08)	16.4(3.4)					
O VI	2.633161	13.26(0.07)	6.7(1.1)					
S VI	2.633173	12.74(0.06)	8.5(1.5)					
O VI	2.633486	13.03(0.16)	7.8(2.1)					
O VI	2.633766	13.40(0.05)	10.1(1.2)					
O VI	2.634119	13.18(0.05)	12.7(1.6)		14.66(0.07)[c]			
Si IV		13.88(0.02)[b]			14.18(0.40)[b]			

[a] From Lopez et al. (1999). [b] Column density integrated over all fitted velocity components. [c] AODM value.

Appendix A: Associated systems

The following three systems also have clear detections of O VI but their redshifts are within $v < 3000$ km s^{-1} of the systemic redshift of the QSO, so we regard them as "associated" systems (e.g., Barlow & Sargent 1997). For purposes of completeness, we briefly describe them here, but do not consider them in our photoionization models. Figures A.1 to A.3 show observed transitions of H I, C IV, and O VI plotted in velocity scale with respect to arbitrary redshifts. It is important to note that the line-of-sight separation, S, is computed in each case assuming that the redshift is purely cosmological, i.e., S is an upper limit if the absorption is produced in outflowing material.

$z = 2.300$, $S = 100$ pc This system lies $v = 1\,800$ km s^{-1} from the systemic redshift of HE1104-1805. We fitted 5 velocity components to the O VI systems along the A line-of-sight. The 1037 transition appears underfitted due to – we believe – shallow absorption by H I interlopers. Despite this caveat, a misaligment between O VI and C IV becomes clear in the 3 bluemost velocity components. Observations of a similar associated system have led Ganguly et al. (2006) to postulate different gas phases with distinct degrees of ionization. When comparing with QSO B, C IV shows transverse structure while the O VI does not, which supports the scenario of different gas regions.

This system is also observed in Si IV, Si III, and C III (not shown in the figure) and is thus particularly well suited for studying physical conditions of the absorbing gas. Assuming the QSO ionizes each of the individual clouds, the size information provided by the two lines-of-sight can give important constraints to the conditions and location of the absorbers within the QSO host galaxy.

$z = 2.315$, $S = 25$ pc This system lies only $v = 450$ km s^{-1} from the systemic redshift of HE1104-1805. All transitions appear identical between the two LOS. In particular, the O VI is weak and the doublet lines have the proper strength ratio.

$z = 2.777$, $S = 70$ pc This system lies $v = 2\,400$ km s^{-1} from the systemic redshift of RX J0911.4+0551 and shows transitions of O VI, C IV, N V, and C III (the latter two are not shown in Fig. A.3). The system is composed of two "clumps" of C IV clouds around $v = 0$ and $v = 150$ km s^{-1}. Only for the bluemost of them can a clear identification of O VI be made. This clump, however, shows no H I, which appears only at the redshift of the redmost components. In the figure we plot the two H I (unsaturated) transitions used to constrain $N_{\rm H\,I}$ in A. These transitions are too noisy in B to perform a fit but comparison of low order (saturated) Lyman lines suggests the $N_{\rm H\,I}$ in B should be similar as in A.

The fits attempted to the metal line profiles show clearly that the O VI doublet lines in the blue components do not show the proper strength ratio, and the same is true for N V and C IV. This effect, seen along *both* LOS, is only evident in the blue components; the two redmost C IV lines near $v = 150$ km s^{-1} can perfectly be fitted.

Anomalous ratios in associated systems have been interpreted as produced by absorbing clouds that do not fully cover the background continuum emission region of the QSO (Barlow & Sargent 1997). However, incomplete coverage would be surprising in our case given the similar column densities in O VI and C IV along LOS A and B, separated by much larger distances than the size of the continuum source (the same applies if the excess flux is due to the unresolved lensed images). The facts that the effect is observed along both LOS and that the red clump does not show anomalous ratios in neither LOS rule out two other possible explanations namely, emission by the lensing galaxy or a bad continuum placement.

Table A.1. Associated O VI systems.

Ion	z	log N(A)[a]	log N(B)[a]	QSO
H I	2.300	16.36(0.23)[b]	16.53(0.23)[a]	HE1104-1805
C IV		14.01(0.02)	14.32(0.02)	
O VI		14.69(0.07)	14.73(0.03)	
H I	2.314	15.80(0.01)	15.33(0.04)	HE1104-1805
C IV		12.77(0.01)	12.82(0.01)	
O VI		13.32(0.02)	13.38(0.04)	
H I	2.776	15.85(0.05)	...	RX J0911.4+0551
C IV		14.10(0.03)	14.20(0.10)	
O VI		14.77(0.02)	14.75(0.03)	

[a] Total column densities. [b] From Lopez et al. (1999).

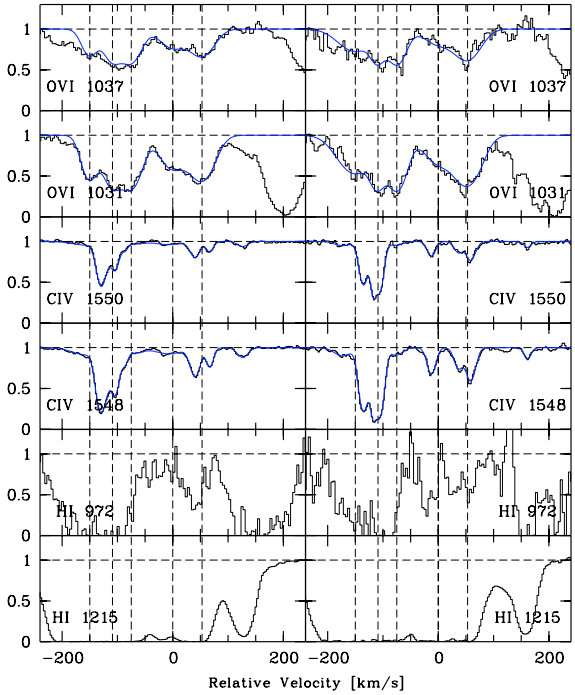

Fig. A.1. Associated system in HE1104-1805 at $z = 2.300$. Panels and symbols as for Fig. 3, but for $z = 2.298472$, $z = 2.298920$, $z = 2.299304$, $z = 2.300127$, and $z = 2.300711$.

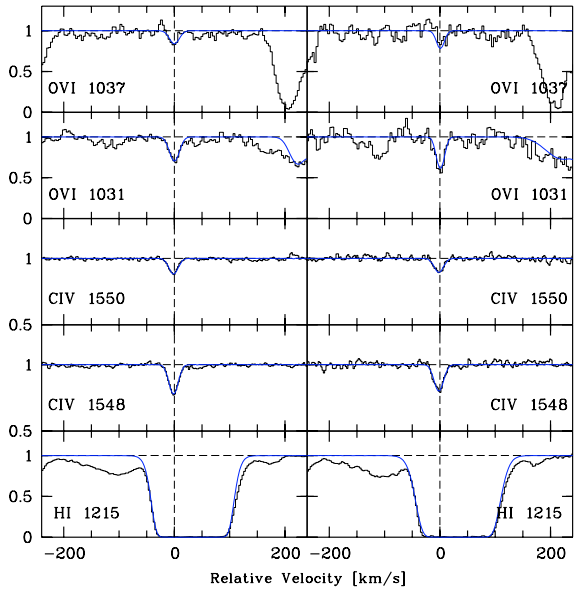

Fig. A.2. Associated system in HE1104-1805 at $z = 2.314$. Panels and symbols as for Fig. 3, but for $z = 2.314201$.

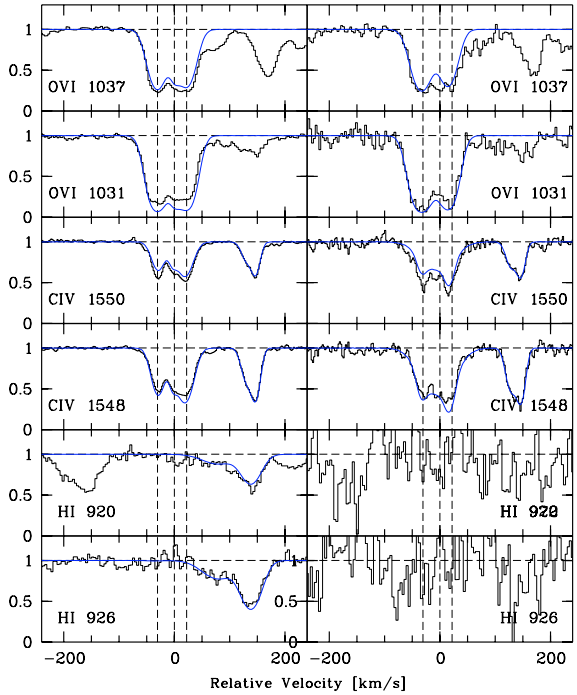

Fig. A.3. Associated system in RX J0911.4+0551. Panels and symbols as for Fig. 3, but for $z = 2.776014$, $z = 2.776399$, and $z = 2.776677$.